RESEARCH PAPER

# Eudragit RS100 nanoparticles for sustained release of Cefpodoxime Proxetil: preparation, pharmaceutical characterization, and *in-vitro* drug release studies

***Jaya Verma [1], Saurabh Shekhar [1], Monika [1], Vikas Jhawat [1], Mahima Chauhan [1], Sonali [2], Rahul Pratap Singh*[1]***

*[1] Department of Pharmacy, School of Healthcare and Allied Sciences, GD Goenka University, Sohna, Gurugram Road, Haryana, India*
*[2] Department of Pharmacy, Guru Teg Bahadur Hospital, Dilshad Garden, Delhi, India*

## ABSTRACT

***Objective(s):*** The primary objective of this study was to develop a sustained-release formulation of cefpodoxime proxetil (CP) using the polymer Eudragit RS 100 (ERS100).

***Materials and Methods:*** Pluronic F127 (PF127) was incorporated as an amphiphilic surfactant to enhance product stability. Preformulation evaluations, including UV-visible spectroscopy and Fourier-transform infrared spectroscopy (FTIR), were performed to assess the compatibility of the drug, polymer, and their 1:1 mixture. Nanoparticles were formulated using the solvent evaporation technique, followed by continuous stirring of the emulsion during the removal of the organic solvent.

***Results:*** The optimized formulation exhibited a particle size of less than 200 nm and an entrapment efficiency of 81.45 ± 0.891% for CP. In vitro drug release studies revealed sustained-release behavior, with the release kinetics best fitting the Higuchi ($R^2$ = 0.9757) and Hixson–Crowell ($R^2$ = 0.9707) models. Stability studies confirmed compliance with ICH guidelines regarding temperature and humidity conditions. These findings underscore the potential of CP-loaded nanoparticles as efficient carriers for sustained drug delivery, particularly targeting lung tissues.

***Conclusion:*** The developed ERS100-based CP nanoparticles offer promising therapeutic benefits, including improved patient adherence through extended drug release intervals.

***Keywords:*** *Cefpodoxime proxetil; Drug delivery systems; Drug stability; Eudragit RS100; Nanoparticles; Pluronate F127.*

**How to cite this article**

*Verma J, Shekhar S, Monika , Jhawat V, Chauhan M, Sonali, Singh RP. Eudragit RS100 nanoparticles for sustained release of Cefpodoxime Proxetil: preparation, pharmaceutical characterization, and in-vitro drug release studies. Nanomed J. 2026; 13(1): 210-223. DOI: 10.22038/NMJ.2025.82111.2045*

## Graphical Abstract

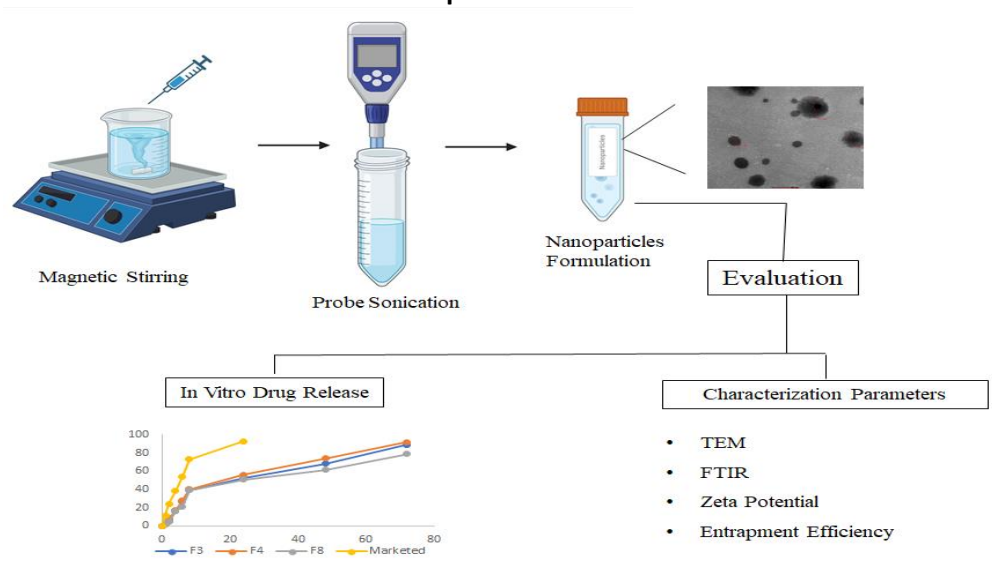


* *Corresponding author(s):* Rahul Pratap Singh, Professor, Department of Pharmacy, School of Healthcare and Allied Sciences, GD Goenka University, Sohna, Gurugram Road, Haryana, India. E-mail: *anuraza2009@gmail.com*.

Note. This manuscript was submitted on August 25, 2024; approved on June 30, 2025.

## INTRODUCTION

The primary challenge in treating pneumonia lies in the global rise of antibiotic resistance. Prolonged antibiotic use may also contribute to systemic toxicity. Cefpodoxime proxetil (CP), a Biopharmaceutics Classification System (BCS) Class IV drug, is characterized by poor solubility and low permeability. It faces multiple limitations, including limited bioavailability (~50%), increased risk of toxicity, antibiotic resistance, and multidrug resistance (MDR). A promising advancement in CP delivery involves its encapsulation within Eudragit RS 100 (ERS100) nanoparticles— a biocompatible polymer system designed to enhance the drug's pharmacokinetic profile. This novel formulation offers a controlled release mechanism, allowing for sustained and consistent therapeutic drug concentrations at the infection site. Such targeted and prolonged delivery is especially crucial for effectively managing lung infections, where conventional administration routes often fail to deliver optimal results.

In recent years, nanoparticles have garnered considerable attention due to their efficient, precise, and targeted delivery of therapeutic agents across a wide range of applications, including disease treatment and diagnostics [1]. These colloidal, nano-sized particles can modify the physicochemical properties of therapeutic compounds by reducing particle size to the nanoscale and enhancing stability in both in vitro and in vivo environments. The choice of polymer plays a pivotal role in the development of effective drug delivery systems [2]. A variety of polymers have been employed in nanoparticle fabrication. Among them, Eudragit RS100 (ERS100) is a biocompatible, non-biodegradable, and time-dependent synthetic polymer that enables sustained drug release through its permeability, which is regulated by quaternary ammonium groups [3]. Eudragit RS100 is a copolymer composed of ethyl acrylate and methyl methacrylate, with a low proportion of methacrylic acid ester containing quaternary ammonium groups. This polymer can be strategically engineered for targeted lung therapy. Due to its cationic nature, it exhibits strong electrostatic interactions with negatively charged lung epithelial cells, thereby enhancing adhesion to the mucosal surfaces of the respiratory tract. These cationic groups further facilitate cellular uptake through electrostatic attraction, thereby prolonging the drug's residence time at the target site [4,5]. However, the gastrointestinal (GI) tract and intestines impose several physiological barriers that hinder effective therapeutic delivery via the oral route, often resulting in reduced bioavailability and suboptimal clinical outcomes. To address these challenges, various amphiphilic surfactants have been employed in the development of polymeric nanoparticles. Among them, Pluronic F127 (PF127) has gained significant attention in biomedical and pharmaceutical applications due to its distinctive amphiphilic structure, which allows it to serve effectively as a drug delivery vehicle. Recent advancements include the formulation of PF127-based mixed polymeric nanoparticles, where it is combined with other polymers to enhance nanoparticle stability and extend circulation time. Another promising strategy involves conjugating PF127 with different types of nanoparticles to improve targeting efficiency and reduce systemic clearance rates [6]. Based on these properties, it is hypothesized that the combination of ERS100 and PF127 in nanoparticle formulation may enable sustained release of CP, potentially leading to improved clinical outcomes. It is hypothesized that ERS100 would offer a high surface area for efficient encapsulation of CP within the nanoparticle core. At the same time, PF127 would aid in overcoming the physiological barriers of the intestinal tract by enhancing the drug's solubility and permeability across the intestinal membrane [7].

Cefpodoxime proxetil (CP) is a third-generation cephalosporin antibiotic known for its broad-spectrum antimicrobial activity, particularly against *Enterobacteriaceae*, *Streptococci*, and *Staphylococcus aureus*. These pathogens are commonly associated with a wide range of infections, from mild skin conditions to severe diseases such as pneumonia and meningitis [8]. Following administration, CP is metabolized into its active form, cefpodoxime, which exhibits high affinity for penicillin-binding protein 3 (PBP3)—a key enzyme involved in the terminal stages of peptidoglycan synthesis in the bacterial cell wall. By binding to PBP3, cefpodoxime disrupts the cross-linking of peptidoglycan strands, an essential process for maintaining cell wall integrity [9]. This disruption compromises the bacterial cell wall, ultimately leading to cell lysis and death [10].

In this study, we report the development of CP-loaded Eudragit RS100 (ERS100) nanoparticles, engineered for sustained drug delivery to lung tissue, offering a potential breakthrough in the treatment of pneumonia by overcoming conventional drug delivery barriers [11,12]. It is hypothesized that the sustained release of CP from these nanoparticles can significantly enhance drug accumulation in lung tissues, thereby improving

therapeutic outcomes. To assess the compatibility between the drug and polymer, Fourier-transform infrared spectroscopy (FTIR) was employed for detailed chemical analysis of molecular interactions and bonding. The nanoparticle formulations were thoroughly characterized in terms of average particle size, polydispersity index (PDI), zeta potential, encapsulation efficiency, and in vitro drug release behavior. Additionally, transmission electron microscopy (TEM) was used to examine the surface morphology and structural integrity of the optimized nanoparticles. Stability studies were conducted in accordance with ICH guidelines to evaluate the long-term physicochemical stability of the developed formulations.

## MATERIALS AND METHODS

### *Materials*

Cefpodoxime proxetil (CP) was kindly provided as a gift sample by Sun Pharmaceutical Industries, Gurugram, Haryana, India. Eudragit RS100 was procured from Evonik Nutrition & Care GmbH, Germany. Pluronic F127 (PF127) was obtained from Sigma-Aldrich Chemical Pvt. Ltd., Burlington, MA, USA. Methanol, potassium dihydrogen phosphate, disodium hydrogen phosphate, and sodium chloride were purchased from Sisco Research Laboratories (SRL) Pvt. Ltd., Mumbai, India. All other chemicals and reagents used in the study were of analytical grade.

### *Methods*

#### *FTIR spectroscopy*

Fourier-transform infrared (FTIR) spectroscopy was performed to evaluate potential interactions between CP and ERS100. The spectra of pure CP, pure ERS100, and their physical mixture were recorded using a Bruker Alpha FTIR spectrophotometer (Bruker, Germany). Measurements were carried out over a wavelength range of 3500–690 $cm^{-1}$, with each sample subjected to 10 scans within this range [13,14].

#### *Preparation of calibration curve*

To construct the calibration curve for CP, 10 mg of the drug was initially dissolved in a small volume of methanol (used as a cosolvent), with complete dissolution achieved through 1 minute of sonication. The resulting solution was then diluted with phosphate-buffer saline (PBS) (pH 7.4) to prepare a stock solution with a concentration of 100 µg/mL. Subsequently, 1 mL of this stock solution was further diluted with phosphate buffer (pH 7.4) to a final volume of 10 mL. Serial dilutions were then prepared to obtain concentrations of 10, 15, 20, 25, and 30 µg/mL. The absorbance of each solution was measured at 232 nm using a UV-visible spectrophotometer, and the corresponding calibration curve was plotted [15]. A separate calibration curve was also prepared using distilled water as the diluent instead of PBS.

#### *Drug solubility determination*

The solubility of CP was determined in distilled water, methanol, and PBS (pH 7.4) at 25 °C using the shake-flask method [16]. Saturated solutions were prepared by adding an excess amount of the drug to each solvent individually, followed by shaking in a water bath shaker for 24 hours to ensure complete dissolution and equilibrium. After the incubation period, the mixtures were filtered through a 0.45 µm membrane filter to remove undissolved particles. The filtrates were appropriately diluted, and drug concentrations were quantified using a UV-visible spectrophotometer.

#### *Partition coefficient*

The partition coefficient (Log P) of CP was determined to evaluate the drug's distribution between a hydrophobic (n-octanol) and a hydrophilic (aqueous) phase. Equal volumes (50 mL each) of n-octanol and distilled water were mixed with a known concentration of CP. The mixture was vigorously shaken and then allowed to reach equilibrium at room temperature [17]. Following phase separation, the concentration of CP in each phase was quantified using a UV-visible spectrophotometer. The partition coefficient (Log P) was calculated using the following formula:

$$Log\ P = \frac{Drug\ conc.\ in\ octanol}{Drug\ conc.\ in\ water}$$

#### *Preparation of nanoparticles*

CP-loaded nanoparticles were prepared using the solvent evaporation method (Table 1). Briefly, 25 mg of CP and Eudragit RS100 (ERS100) were dissolved in 7 mL of methanol. This organic phase was then added dropwise to 15 mL of an aqueous Pluronic F127 (PF127) solution, stirred continuously at 600 rpm, to form an oil-in-water (O/W) emulsion [18]. The organic-to-aqueous phase ratio was maintained at approximately 1:2. After initial mixing, the emulsion was stirred at a reduced speed of 250 rpm for 10 minutes. Subsequently, the emulsion was subjected to ultrasonication using an ultrasonic probe (Ultrasonic Processor UP200Ht, Hielscher Ultrasonics, Germany) at 60% amplitude for 8 minutes to reduce droplet size and promote nanoparticle formation [19]. Methanol was then

removed using a rotary evaporator (Rotavapor® R100, Buchi, Switzerland). The resulting dispersion was filtered through a 0.45 µm PVDF syringe filter and then centrifuged at 7000 rpm for 40 minutes at 4°C using a Remi C23 Plus Refrigerated Centrifuge (Mumbai, India). The collected pellet was washed two to three times with double-distilled water. To ensure uniform redispersion, 5 mL of freshly prepared 0.1 M PBS (pH 7.4) was added. Residual solvent was further removed using rotary evaporation under a pressure of 72 mbar at a boiling point of 100 °C. Finally, the purified nanoparticles were stored in PBS (pH 7.4) until further use to maintain their stability [20].

Table 1. Formulae of eudragit RS 100 nanoparticle preparations F1 to F14: Eudragit RS100 nanoparticles formulations with different conc. of polymer and surfactant compositions

| Formulation | CP (in mg) | ERS100 (in mg) | PF127 (in mg) |
|---|---|---|---|
| F1 | 25 | 86.4 | 0.100 |
| F2 | 25 | 64.5 | 0.050 |
| F3 | 25 | 64.5 | 0.050 |
| F4 | 25 | 50.0 | 0.080 |
| F5 | 25 | 150.0 | 0.050 |
| F6 | 25 | 150.0 | 0.092 |
| F7 | 25 | 84.0 | 0.071 |
| F8 | 25 | 50.0 | 0.071 |
| F9 | 25 | 107.0 | 0.083 |
| F10 | 25 | 50.0 | 0.065 |
| F11 | 25 | 107.0 | 0.050 |
| F12 | 25 | 107.0 | 0.071 |
| F13 | 25 | 86.6 | 0.100 |
| F14 | 25 | 150.0 | 0.092 |

### *Nanoparticle characterization*

#### *Particle size, polydispersity index (PDI), and zeta potential (ζ) measurements*

The mean particle size, polydispersity index (PDI), and zeta potential (ζ) of the developed nanoparticles were determined using Photon Correlation Spectroscopy (PCS) with a Litesizer™ 500 analyzer (Anton Paar GmbH, Graz, Austria) [21].

#### *Transmission electron microscopy (TEM)*

The surface morphology of the developed nanoparticles was examined using a transmission electron microscope (Talos F200X G2 TEM, Thermo Fisher Scientific, USA). A drop of the nanoparticle suspension was placed onto a 200-mesh carbon-coated copper grid (3 mm in diameter) and air-dried for 30 minutes to allow solvent evaporation. After drying, the sample was imaged using the TEM system to observe the shape and surface characteristics of the nanoparticles [22,23].

#### *Drug entrapment efficiency determination*

The drug entrapment efficiency of the formulated CP-loaded ERS100 nanoparticles highlights their significant capacity to encapsulate and retain the drug within the polymeric matrix [24,25]. Briefly, a 0.5 mL aliquot of CP-loaded ERS100 nanoparticles was transferred to a round-bottom flask and subjected to solvent evaporation until dryness using a rotary evaporator operated at a pressure of 72 mbar and a temperature of 70 °C. The dried residue was then reconstituted in 5 mL of PBS (pH 7.4) and sonicated to disrupt the nanoparticles. Following sonication, the sample was centrifuged at 7000 rpm for 10 minutes at 4 °C. The resulting supernatant was collected and diluted to a final volume of 5 mL with PBS (pH 7.4). The absorbance was measured at 234 nm using a UV-visible spectrophotometer [26]. The percentage of CP entrapment efficiency was calculated using the following formula:

$$\%\ Drug\ encapsulation\ efficinecy = \frac{\frac{Total\ drug\ amount}{in\ nanoparticles\ fabrication}}{\frac{Total\ drug\ amount\ added}{during\ nanoparticles\ fabrication}} * 100$$

#### *In-vitro drug release studies*

The in vitro drug release profile of CP-loaded ERS100 nanoparticle formulations was evaluated using the dialysis bag diffusion technique. To compare release behavior, free CP suspension in PBS(Ph 7.4) was used as a control [27]. Briefly, 250 µg of CP—either in nanoparticle form or as a free suspension—was separately placed into dialysis bags with a molecular weight cut-off (MWCO) of 1 kDa. The sealed bags were immersed in 100 mL of PBS (pH 7.4) and incubated in a water bath shaker maintained at 37 ± 0.5 °C with continuous agitation at 100 rpm for up to 72 hours. To maintain sink conditions, 5 mL of release medium was withdrawn at predetermined intervals and immediately replaced with an equal volume of fresh PBS. The withdrawn samples were filtered through a 0.45 µm syringe filter before analysis. The drug concentration in each sample was quantified by measuring the absorbance at 234 nm using a UV-visible spectrophotometer. All measurements were performed in triplicate, and results were reported as mean values with standard deviations [28].

Then, the cumulative drug release data were calculated and fitted to various release kinetic models, *i.e.,* zero order ($Q=Q_0+k_0t$), first order ($dC/dt=-k_1t$), Higuchi's model ($Q=kt^{0.5}$), Korsmeyer–Peppas ($F=M_t/M_\infty=k_t^n$) and Hixson–Crowell model ($W_0^{1/3} - W_t^{1/3} = K_{HC}t$) [29]. Where are Q represents the amount of drug released from the

nanoparticles, $Q_0$ shows the amount of drug initially present in the solution, $k_0$ denotes the rate constant for zero order expressed in conc./time, and t is time, $k_1$ represents the first-order rate constant expressed in time$^{-1}$, F is the fraction of drug release at time 't', $M_t$ shows the amount of drug released at time 't' $M_\infty$ mentions the total amount of drug in dosage form, K denotes the Korsmeyer–Peppas constant, n is the diffusion or release exponent, W0 presents the initial amount of drug, Wt shows the amount of drug at any time t, and $K_{HC}$ expresses the Hixson-Crowell constant [30].

### *Stability studies*

To assess product stability, the developed nanoparticles were stored under controlled environmental conditions, including refrigerated (5 ± 2°C, 60% ± 5% RH), room temperature (25 ± 2°C, 35% ± 5% RH), and accelerated storage conditions (40 ± 2°C, 75 ± 5% RH) under ICH guidelines. The effect of these storage conditions on particle size, polydispersity index (PDI), and encapsulation efficiency was evaluated at three time points: initially (0 months), after 1 month, and after 3 months of storage [31,32].

### *Statistical analysis*

All experimental results are presented as mean ± standard deviation (SD) of three independent measurements, analyzed using GraphPad Prism software. Statistical significance was assessed using the unpaired t-test and one-way analysis of variance (ANOVA), followed by Tukey's multiple comparison test where appropriate.

## RESULTS AND DISCUSSION

### *FTIR spectroscopy*

The FTIR spectra presented in Figure 1(A–C) display the characteristic functional groups of the drug, polymer, and their physical mixture at a 1:1 ratio. In Figure 1(A), distinctive peaks CP are observed, particularly within the 2800–3000 cm$^{-1}$ range, indicating the C–H stretching vibrations. Peaks in the region of 1700–1750 cm$^{-1}$ suggest the presence of carbonyl (C=O) groups, while those between 1000–1300 cm$^{-1}$ correspond to C–O stretching vibrations, typically associated with ethers, alcohols, or esters [33].

Figure 1(B) shows peaks indicative of residual double bonds, particularly in the 1600–1650 cm$^{-1}$ region, suggesting the presence of carbon–carbon double bonds within the polymer structure. Additionally, peaks observed in the 2800–3000 cm$^{-1}$ range correspond to C–H stretching vibrations in the polymer's alkyl chains. In the FTIR spectrum of the physical mixture, characteristic peaks around 1000–1300 cm$^{-1}$ represent ester functional groups of the polymer, while a distinct peak at 1754 cm$^{-1}$ indicates the presence of carbonyl (C=O) groups. Analysis confirms the presence of distinctive peaks from both the drug and the polymer (Eudragit RS100) across all spectra [34]. Furthermore, the absence of significant shifts or disappearance of functional group peaks suggests that only physical interactions occurred between the drug and excipients, with no evidence of chemical interaction

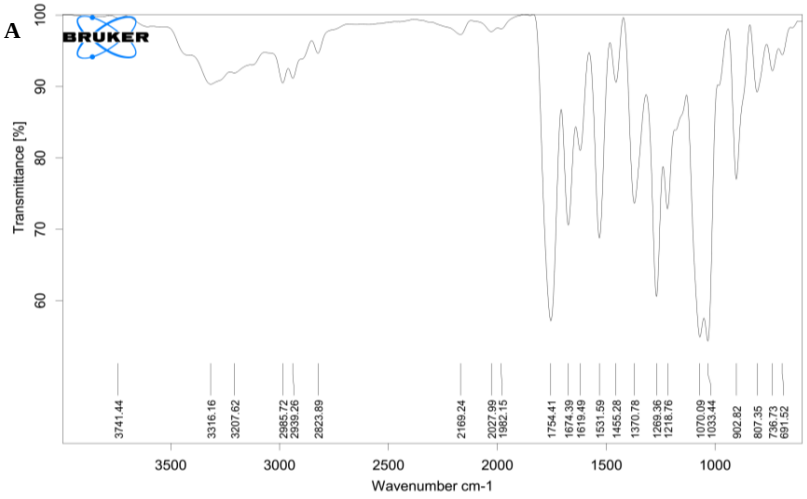

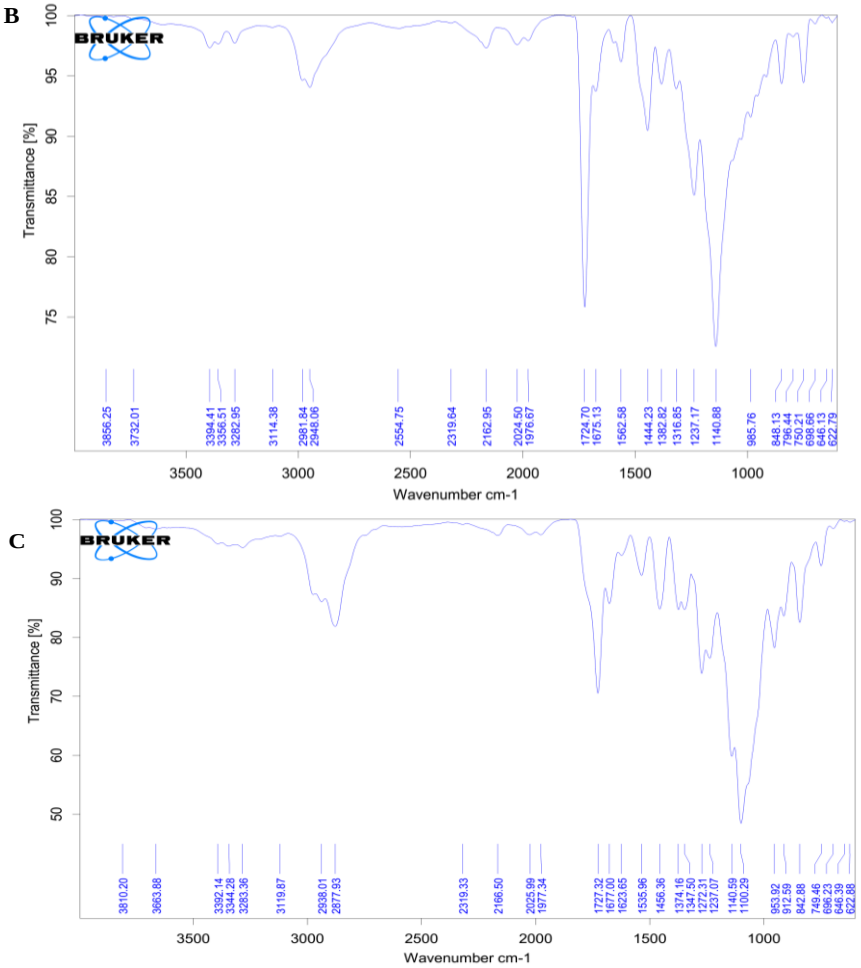


Fig. 1. FTIR spectrum graphs for (A) CP, (B) ERS100, and (C) a mixture of CP and ERS100 at ratio 1:1.

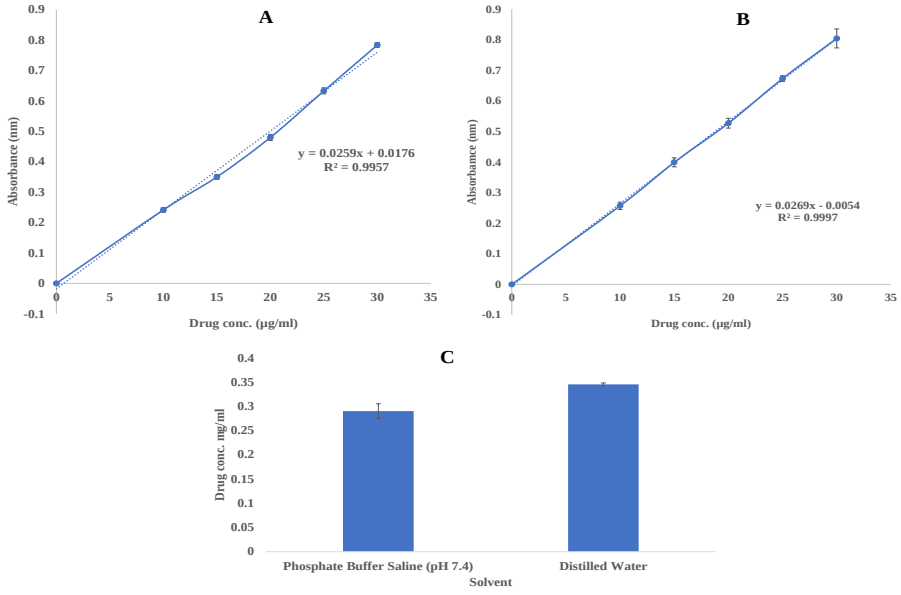


Fig. 2. CP calibration curves in different solvents, i.e., A) phosphate buffer saline at pH 7.4, B) distilled water, at drug concentrations ranging from 10 to 30 µg/ml, and C) drug solubility in phosphate buffer saline pH 7.4 and distilled water.

***Preparation of calibration curve***

Figures 2A and 2B illustrate the calibration curves of CP in freshly prepared PBS pH 7.4) and distilled water, respectively. Methanol was selected as the solvent for reference due to its high solubility for CP and the sharp, symmetric peak profiles it produced, which facilitated accurate quantification. The UV-visible absorbance maxima of CP were examined in various solvents, including water and PBS, confirming that the absorption peaks and overall spectral profiles were comparable across media. Although methanol provided superior quantification at lower concentrations, the consistency in peak shape across methanol, water, and octanol validated the calibration approach in different environments. The linear relationship between absorbance and concentration for CP in PBS and distilled water was established using the Beer–Lambert law. The calibration curves showed good linearity in the concentration range of 10–30 µg/mL. Concentration values were determined from triplicate measurements, confirming the method's reproducibility. These findings support the suitability of UV-visible spectrophotometry as a simple and reliable technique for constructing CP calibration curves.

***Drug solubility determination***

Cefpodoxime proxetil (CP) is a poorly water-soluble drug classified under the Biopharmaceutics Classification System (BCS) Class IV. Such compounds pose significant challenges in pharmaceutical formulation due to their low aqueous solubility, which is typically associated with poor dissolution behavior and limited oral bioavailability. The solubility of CP in PBS (pH 7.4) was found to be 0.290 ± 0.015 mg/mL, which is lower than its solubility in distilled water (0.345 ± 0.003 mg/mL). This difference can be attributed to the ionic strength and specific ion–solute interactions present in the PBS. However, a significant enhancement in solubility was achieved through ultraprobe sonication. This technique improves solubility by facilitating the complete adsorption or co-precipitation of polymers onto drug particles, thereby acting as solubilizing agents and enhancing particle dispersion and wettability. Furthermore, sonication exerts mechanical shear and attrition forces, leading to particle size reduction. Smaller particles possess a greater surface area-to-volume ratio, which enhances the dissolution rate by increasing the contact area between the drug and solvent and lowering the energy barrier to dissolution [35]. To better replicate physiological conditions, no surfactants or solubility enhancers were employed during solubility testing. Although surfactants such as Tween 80 or sodium dodecyl sulfate (SDS) are commonly used to increase solubility, their presence can artificially accelerate the dissolution rate, potentially skewing the in vitro release profile.

***Partition coefficient***

The partition coefficient (log P) of CP, defined as the ratio of its concentration in a hydrophobic phase (n-octanol) to that in a hydrophilic phase (aqueous buffer), serves as an indicator of the drug's lipophilicity and potential bioavailability. In this study, the concentration of CP in the octanol phase was determined to be 1.61 mg, while its concentration in the aqueous phase was 0.389 mg.

The partition coefficient (log P) is given by:

$$\textit{Partition coefficient}\ (\log P) = \frac{\textit{Concentration in octanol}}{\textit{Concentration in water}}$$

Substituting the values given:

$$\textit{Partition coefficient}\ (\log P) = \frac{1.61}{0.389}$$

The higher concentration of CP in the octanol phase indicates its greater affinity for lipophilic environments, which aligns with its known physicochemical properties. This lipophilic tendency suggests enhanced potential for membrane permeability, a critical factor influencing oral absorption and systemic bioavailability [36]. The experimentally determined log P value of CP was 4.17, further confirming its lipophilic nature and potential for passive diffusion across lipid bilayers.

***Preparation of nanoparticles***

Among all tested formulations, F4 exhibited the smallest mean particle size (203.35 ± 15 nm), which is advantageous for drug delivery applications. Smaller particle sizes are generally associated with enhanced dissolution rates and improved oral bioavailability. In contrast, other formulations demonstrated significantly larger particle sizes, such as F14 (798.22 ± 48 nm) and F6 (584.47 ± 22 nm), which may negatively impact dissolution and subsequent drug absorption. The polydispersity index (PDI) of F4 was 0.410 ± 0.02, indicating a relatively narrow particle size distribution and suggesting

uniformity in particle morphology. A lower PDI is preferred, as it reflects greater stability and consistency of the formulation. By comparison, several other formulations displayed higher PDIs, including F5 (0.632 ± 0.03) and F14 (0.619 ± 0.03), which may contribute to formulation instability and variability in performance. Formulation F4 demonstrated the highest drug encapsulation efficiency (EE) at 81.65 ± 0.812%, indicating a greater proportion of the drug was successfully incorporated into the delivery system, which is favorable for enhancing therapeutic efficacy [37]. In contrast, other formulations such as F5 (71.09 ± 0.810%) and F14 (70.76 ± 0.866%) exhibited significantly lower %EE values, suggesting reduced drug loading and potentially less effective delivery. Larger particle sizes in specific formulations also resulted in a cloudy appearance, which is generally undesirable in pharmaceutical preparations due to aesthetic and stability concerns. Moreover, high polydispersity index (PDI) values are associated with inconsistent drug release profiles, which may lead to unpredictable therapeutic outcomes. In summary, formulation F4 outperformed the remaining thirteen formulations due to its smaller particle size, narrower particle size distribution, and superior encapsulation efficiency. These attributes collectively contribute to enhanced formulation stability, improved drug bioavailability, and more efficient drug delivery performance.

***Characterization of ERS100 nanoparticles***

The particle size of nanoparticles plays a critical role in determining their biological distribution, cellular uptake, and drug release kinetics. Smaller nanoparticles typically exhibit enhanced tissue penetration, whereas larger particles tend to remain in systemic circulation for extended periods. The zeta potential reflects the surface charge of nanoparticles and serves as an indicator of colloidal stability; higher absolute values indicate better suspension stability. The polydispersity index (PDI) represents the uniformity of particle size distribution, with lower values indicating a more homogeneous population—an essential factor for consistent drug delivery and reproducible release behavior. Among the tested formulations, F4 exhibited the smallest particle size and the highest negative zeta potential, suggesting superior stability and a more controlled release profile compared to F3 and F8.

***Particle size, polydispersity index (PDI), and zeta potential (ζ) measurements***

The particle size, polydispersity index (PDI), and zeta potential (ζ) of the ERS100 nanoparticles were evaluated, as presented in Table 2 and Figure 3 (A–C). The optimized formulation, F4, demonstrated favorable physicochemical properties, including a mean particle size of 205 ± 0.628 nm, a zeta potential of −38.5 mV, and a PDI of 0.410 ± 0.076, indicating good colloidal stability and a moderately uniform particle distribution.

***Transmission electron microscopy (TEM)***

Figure 3D illustrates the spherical shape and smooth surface morphology of the nanoparticles, as observed through Transmission Electron Microscopy (TEM) analysis using the TALOS model. TEM provided both qualitative and quantitative insights into the nanoparticle structure, including particle size distribution, aspect ratio, and surface characteristics [38]. The images revealed a distinct dark core, corresponding to the drug, surrounded by a lighter polymeric matrix, indicating successful encapsulation. The average particle size observed via TEM was consistent with the results from dynamic light scattering, falling within the ~200 nm range.

***Drug entrapment efficiency determination***

Table 2 and Figure 3C present the encapsulation efficiency of the ERS100 nanoparticle formulations. The encapsulation efficiencies for formulations F3, F4, and F8 were found to be 77.03 ± 0.712%, 81.65 ± 0.812%, and 81.74 ± 0.612%, respectively. These results indicate that the concentrations of ERS100 and PF127 were precisely optimized to achieve maximal drug entrapment. The high encapsulation efficiency observed in these formulations underscores their potential for the sustained delivery of CP, which is essential for effective management of various infectious diseases [39]. In particular, the elevated efficiencies confirm that the formulation parameters were appropriately fine-tuned, enabling the nanoparticles to effectively encapsulate and deliver the therapeutic agent. Such efficient encapsulation is crucial for ensuring an adequate drug concentration at the target site, thereby enhancing therapeutic efficacy while minimizing systemic side effects.

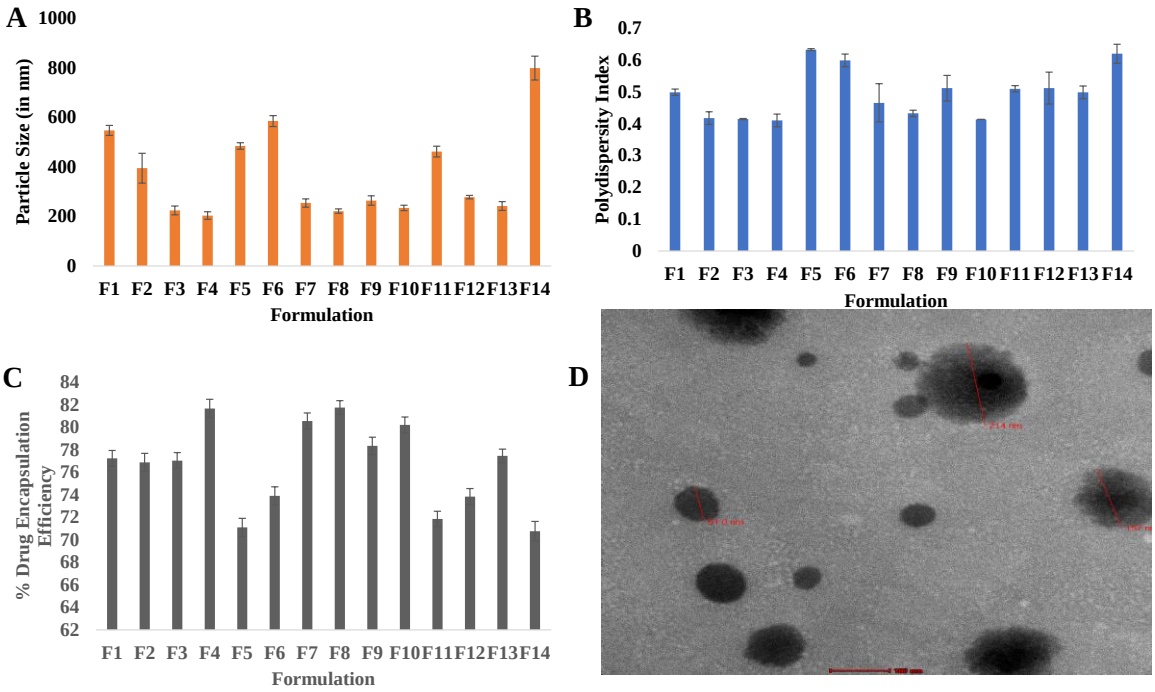


Fig. 3. (A) Particle size, (B) polydispersity, (C) drug encapsulation efficiency of developed eudragit RS 100 nanoparticles, and (D) TEM image of F4 nanoparticle formulation at scale bar 200nm

Table 2. Particle size, polydispersity index, and drug encapsulation efficiency of eudragit RS100 nanoparticles

| Formulation | Particle size (length; nm) (mean ± S.D.*)[a] | Polydispersity index (mean ± S.D.*)[a] | Drug Encapsulation efficiency (%) (mean ± S.D.*)[a] |
|---|---|---|---|
| F1 | 546.77 ± 20 | 0.498 ± 0.01 | 77.22 ± 0.701 |
| F2 | 394.42 ± 60 | 0.417 ± 0.02 | 76.87 ± 0.805 |
| F3 | 223.76 ± 18 | 0.414 ± 0.002 | 77.03 ± 0.712 |
| F4 | 203.35 ± 15 | 0.410 ± 0.02 | 81.65 ± 0.812 |
| F5 | 483.98 ± 13 | 0.632 ± 0.03 | 71.09 ± 0.810 |
| F6 | 584.47 ± 22 | 0.598 ± 0.02 | 73.89 ± 0.811 |
| F7 | 253.82 ± 17 | 0.465 ± 0.06 | 80.54 ± 0.712 |
| F8 | 221.11 ± 09 | 0.432 ± 0.01 | 81.74 ± 0.612 |
| F9 | 263.62 ± 19 | 0.511 ± 0.04 | 78.33 ± 0.781 |
| F10 | 234.19 ± 11 | 0.413 ± 0.00 | 80.19 ± 0.705 |
| F11 | 461.37 ± 22 | 0.509 ± 0.01 | 71.85 ± 0.683 |
| F12 | 277.51 ± 07 | 0.511 ± 0.05 | 73.83 ± 0.708 |
| F13 | 241.93 ± 18 | 0.498 ± 0.02 | 77.45 ± 0.604 |
| F14 | 798.22 ± 48 | 0.619 ± 0.03 | 70.76 ± 0.866 |

* n=4 [a] S.D.: Standard deviation (P<0.05).

F1 to F14: Eudragit RS100 nanoparticles formulations with different conc. of polymer and surfactant compositions

### *In-vitro drug release studies*

During the drug release studies, experimental conditions were designed to approximate sink conditions by maintaining a sufficiently high buffer volume-to-drug ratio. The PBS volume was selected based on preliminary solubility assessments, which confirmed that drug solubility did not impose a significant limitation on release. Specifically, the drug was dispersed in 100 mL of PBS at a concentration well below its saturation solubility (0.290 µg/mL), with approximately 190 µg of CP used per 100 mL, thereby ensuring that sink conditions were initially maintained. However, it is acknowledged that ideal sink conditions may not have been sustained throughout the entire duration of the experiment. Figure 4 illustrates the in vitro release profiles of CP from ERS100 nanoparticle formulations. During formulation

optimization, the drug release kinetics of several CP-loaded nanoparticles—specifically F3, F4, and F8—were evaluated in comparison with both the pure active pharmaceutical ingredient (API) and a marketed formulation. Notably, the cumulative release of the marketed product reached 91 ± 0.586% within 8 h. In contrast, the nanoparticle formulations (F3, F4, and F8) exhibited sustained-release behavior, with cumulative drug release ranging from 89.42 ± 0.481% to 92.86 ± 0.406% over 48 h. These findings are graphically represented and highlight the prolonged release capacity of the developed formulations.

The in vitro release data were fitted to various kinetic models, including zero-order, first-order, Higuchi, Hixson–Crowell, and Korsmeyer–Peppas equations. The primary aim was to determine the model that best described the drug release kinetics from the developed formulations. The optimized formulations (F3, F4, and F8) demonstrated sustained-release behavior. Among the tested models, the Higuchi and Hixson–Crowell equations provided the best fit, suggesting that drug release occurred via a combined mechanism of diffusion and matrix erosion. Additionally, favorable adjusted $R^2$ values and suitable exponential release coefficients (n values) were observed, further supporting the applicability of these models to the release profiles. The selection of the most appropriate model was based on statistical parameters, primarily the adjusted $R^2$, which reflects the model's ability to explain variability in the experimental data. These results are summarized in Table 3.

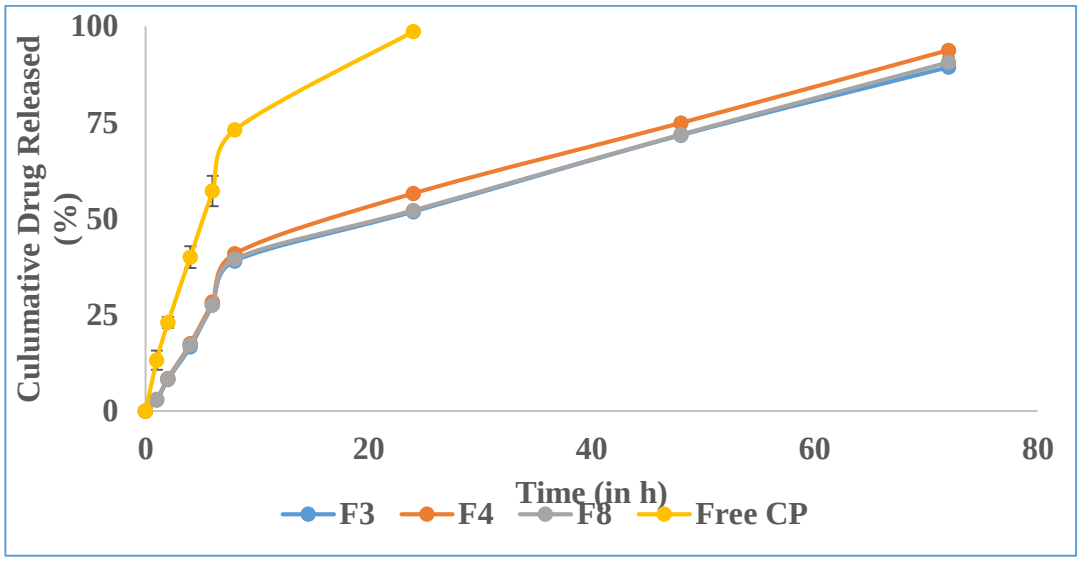


Fig.4. The in-vitro drug release profiles of the CP suspension, and optimized CP-loaded ESR100 nanoparticles (F3, F4, and F8)

Table 3. Kinetic modelling of drug release from the CP formulations

| Formulation | Zero-order Model | First-Order Model | Higuchi Model | Korsmeyer Peppas Model | Hixson Crowell Model |
|---|---|---|---|---|---|
| **F3** | 0.890 | 0.874 | 0.9755 | 0.4938 | 0.9682 |
| **F4** | 0.887 | 0.905 | 0.9753 | 0.4917 | 0.9709 |
| **F8** | 0.893 | 0.873 | 0.9759 | 0.4936 | 0.969 |
| **Free CP** | 0.805 | 0.996 | 0.8053 | 0.3975 | 0.9812 |

Free CP: Conventional CP suspension formulation

F3, F4 and F87: CP loaded ERS100 nanoparticles containing different concentrations of ERS100 and PF127

The linearity of the applied kinetic models outperformed that of alternative models, emphasizing the sustained and diffusion-controlled drug release from matrix-based systems. This release pattern indicates that CP-loaded nanoparticles provide consistent drug release over an extended period, thereby supporting prolonged pharmacological action while minimizing potential side effects [40]. Notably, the Higuchi model provided an excellent fit to the release data, with an exponent value (n) exceeding 0.89, indicative of a super case II transport mechanism. This suggests

that both diffusion and relaxation of the polymer matrix govern the release of CP from ERS100 nanoparticles. The release kinetics are effectively described by a combination of Fickian (diffusion-driven) and non-Fickian (erosion- or swelling-related) mechanisms [41]. While the Higuchi model emphasizes diffusion as the dominant mechanism, the Hixson–Crowell and Korsmeyer–Peppas models provide further support for the involvement of matrix erosion processes. The high adjusted $R^2$ values and consistent n values across formulations confirm that these models reliably capture the sustained-release characteristics of the system, indicating a dual mechanism of diffusion and erosion for effective and controlled drug delivery.

In contrast, the zero-order and first-order models were found to be less suitable for describing the drug release behavior, as they failed to capture the complexity of the observed release mechanisms [42]. The zero-order model assumes a constant rate of drug release. In contrast, the first-order model is based on concentration-dependent kinetics, neither of which adequately reflects the sustained and controlled release profile exhibited by the formulations. Therefore, the Higuchi and Hixson–Crowell models offered a more accurate and comprehensive understanding of the drug release kinetics from the ERS100 nanoparticles. Among all the tested formulations, F4 emerged as the optimized formulation, exhibiting the best goodness of fit to the kinetic models. Specifically, the Higuchi model demonstrated a high correlation coefficient ($R^2$ = 0.977), an exponential value (n = 0.894), and an adjusted $R^2$ of 0.9757 for F4. These results indicate that the F4 formulation aligns most closely with the predicted release behavior, confirming its suitability as the lead candidate for sustained drug delivery.

***Stability studies***

The stability evaluation primarily focused on assessing both the physical integrity of the nanoparticles and the chemical stability of the encapsulated drug. Although drug release rate is a key determinant of therapeutic efficacy, it was not included in the stability analysis, as the primary objective was to determine whether the nanoparticle formulations maintained their structural and chemical integrity over time. Drug release profiles are significantly influenced by external physiological conditions such as pH, enzymatic activity, and solubility in biological fluids—factors that differ substantially from the controlled environmental parameters (e.g., temperature and humidity) employed in stability testing. Therefore, stability studies are designed to confirm the chemical integrity and physical robustness of the formulation. At the same time, drug release profiles are more appropriate for evaluating pharmacokinetic behavior and bioavailability under biological conditions. Stability studies, as detailed in Table 4, provide essential insights into the behavior of the nanoparticles under different storage conditions. Under refrigerated conditions (5 ± 2 °C, 60 ± 5% RH) and room temperature (25 ± 2 °C, 60 ± 5% RH), both particle size and entrapment efficiency (EE) remained relatively stable throughout the study period. In contrast, when exposed to more stringent storage conditions—elevated temperature (40 ± 2 °C) and humidity (75 ± 5% RH)—a noticeable increase in particle size was observed. This change is likely attributable to particle aggregation or clustering, possibly due to enhanced molecular mobility and increased interparticle interactions under these conditions.

Table 4. Stability study of F4: CP loaded ERS100 nanoparticles

| Temp (°C)/RH (%) | Time (months) | Particle size (nm) | Entrapment efficiency (EE)% |
|---|---|---|---|
| Refrigerated temp. (5 ± 2° C, 60% ± 5% RH) | 0 | 205±0.628 | 81±0.812 |
| | 1 | 208±0.608 | 81±0.802 |
| | 3 | 211±0.618 | 80±0.822 |
| Room temp. (25± 2° C, 35% ± 5% RH) | 0 | 209±0.622 | 80±0.813 |
| | 1 | 215±0.610 | 79±0.811 |
| | 3 | 215±0.618 | 79±0.792 |
| Accelerated temp. 40 ± 2°C/75 ± 5% | 0 | 225±0.628 | 80±0.789 |
| | 1 | 231±0.628 | 77±0.782 |
| | 3 | 245±0.628 | 72±0.792 |

Notably, despite the increase in particle size under accelerated conditions, the entrapment efficiency exhibited only minor variation, indicating that the chemical stability of the encapsulated drug was mainly preserved [43]. These findings suggest that although storage conditions may mildly influence the physical characteristics of the nanoparticles, the encapsulation efficiency of the active pharmaceutical ingredient remains broadly stable. Minor changes in particle size did not

significantly impact the drug's retention within the nanoparticle matrix, indicating satisfactory formulation stability over the evaluation period. Future studies will aim to assess drug release profiles in conjunction with stability testing to gain a more comprehensive understanding of formulation performance over time. Preliminary observations also demonstrated that the nanoparticles maintained their structural integrity under various conditions, supporting the expectation that the drug release rate would remain consistent, provided structural stability is preserved.

## CONCLUSION

Nanoparticles developed for therapeutic applications offer several advantageous properties that significantly improve drug delivery systems. These formulations exhibit precisely controlled particle sizes below 200 nm, a critical factor for enhancing colloidal stability, primarily achieved through optimized zeta potential values [44–45]. Transmission Electron Microscopy (TEM) analysis confirmed their consistently spherical morphology, indicating robust structural integrity, which is essential for efficient drug delivery. The optimized formulations—F3, F4, and F8—demonstrated sustained release profiles. Among the various kinetic models evaluated, the Higuchi and Hixson–Crowell models provided the best fit, suggesting that a combination of diffusion and matrix erosion mechanisms governs drug release. The selected kinetic models indicate that drug release from the nanoparticles follows a combined diffusion- and erosion-controlled mechanism, which is essential for maintaining a sustained therapeutic effect. In addition, comprehensive stability assessments confirmed the long-term physical and chemical stability of the formulations, further supporting their suitability for extended shelf-life. Taken together, these findings highlight the potential of nanoparticle-based systems as a promising therapeutic platform. Compared to conventional drug formulations, these nanoparticles offer enhanced efficacy, prolonged drug release, and reduced side effects. Their ability to improve targeted delivery and ensure more consistent therapeutic outcomes underscores their value in advancing modern drug delivery strategies [46].

## AUTHORSHIP CONTRIBUTION

Jaya Verma: Writing – original draft, Investigation. Saurabh Shekhar: Writing – review & editing, Investigation. Mahima Chauhan: Writing – review & editing, Investigation. Monika: Writing – review & editing, Supervision, Conceptualization. Vikas Jhawat: Writing – review & editing, Investigation. Sonali: Writing – review & editing, Investigation. Rahul Pratap Singh: Writing – review & editing, Supervision, Conceptualization.

## CONFICTS OF INTEREST

The authors declare that they have no known competing financial interests or personal relationships that could have appeared to influence the work reported in this paper

## DATA AVAILABILITY

Data will be made available on request.

## REFERENCE


1. Mitchell MJ, Billingsley MM, Haley RM, Wechsler ME, Peppas NA, Langer R. Engineering precision nanoparticles for drug delivery. Nat Rev Drug Discov. 2021;20(2):101-124.
2. Begines B, Ortiz T, Pérez-Aranda M, Martínez G, Merinero M, Argüelles-Arias F, Alcudia A. Polymeric nanoparticles for drug delivery: recent developments and future prospects. Nanomaterials (Basel). 2020;10(7):1403.
3. Zielińska A, Carreiró F, Oliveira AM, Neves A, Pires B, Venkatesh DN, et al. Polymeric nanoparticles: production, characterization, toxicology and ecotoxicology. Molecules. 2020;25(16):3731.
4. Iqbal O, Shah S, Abbas G, Rasul A, Hanif M, Ashfaq M, et al. Moxifloxacin loaded nanoparticles of disulfide bridged thiolated chitosan-eudragit RS100 for controlled drug delivery. Int J Biol Macromol. 2021;182:2087-2096.
5. Cortesi R, Ravani L, Menegatti E, Esposito E, Ronconi F. Eudragit(®) microparticles for the release of budesonide: a comparative study. Indian J Pharm Sci. 2012;74(5):415-421.
6. Akash MS, Rehman K. Recent progress in biomedical applications of pluronic (PF127): pharmaceutical perspectives. J Control Release. 2015;209:120-138.
7. Nedelcu A, Mosteanu O, Pop T, Mocan T, Mocan L. Recent advances in nanoparticle-mediated treatment of inflammatory bowel diseases. Applied Sciences. 2021;11(1):438.
8. Geddes AM. Cefpodoxime proxetil in the treatment of lower respiratory tract infections. Drugs. 1991;42 Suppl 3:34-40.
9. Fulton B, Perry CM. Cefpodoxime proxetil: a review of its use in the management of bacterial infections in paediatric patients. Paediatr Drugs. 2001;3(2):137-158.
10. Xiong MH, Bao Y, Yang XZ, Zhu YH, Wang J. Delivery of antibiotics with polymeric particles. Adv Drug Deliv Rev. 2014;78:63-76.
11. Huh AJ, Kwon YJ. "Nanoantibiotics": a new paradigm for treating infectious diseases using nanomaterials in the antibiotics resistant era. J Control Release. 2011;156(2):128-145.

12. Chu L, Gao H, Cheng T, Zhang Y, Liu J, Huang F, et al. A charge-adaptive nanosystem for prolonged and enhanced in vivo antibiotic delivery. Chem Commun (Camb). 2016;52(37):6265-6268.
13. Sharma A, Keservani R, Dadarwal S, Choudhary Y, Ramteke S. Formulation and in vitro characterization of cefpodoxime proxetil gastroretentive microballoons. Daru. 2011;19(1):33-40.
14. Malik A, Parveen S, Ahamad T, Alshehri SM, Singh PK, Nishat N. Coordination polymer: synthesis, spectral characterization and thermal behaviour of starch-urea based biodegradable polymer and its polymer metal complexes. Bioinorg Chem Appl. 2010;2010:848130.
15. Asnani G, Jadhav K, Dhamecha D, Sankh A, Patil M. Development and validation of spectrophotometric method of cefpodoxime proxetil using hydrotropic solubilizing agents. Pharm Methods. 2012;3(2):117-120.
16. Veseli A, Žakelj S, Kristl A. A review of methods for solubility determination in biopharmaceutical drug characterization. Drug Dev Ind Pharm. 2019;45(11):1717-1724.
17. Bannan CC, Calabró G, Kyu DY, Mobley DL. Calculating partition coefficients of small molecules in octanol/water and cyclohexane/water. J Chem Theory Comput. 2016;12(8):4015-4024.
18. Mostafa GAE, Al-Otaibi YH, Al-Badr AA. Cefpodoxime proxetil. Profiles Drug Subst Excip Related Methodol. 2019;44:1-165.
19. Jana U, Mohanty AK, Manna PK, Mohanta GP. Preparation and characterization of nebivolol nanoparticles using Eudragit® RS100. Colloids Surf B Biointerfaces. 2014;113:269-275.
20. Adibkia K, Javadzadeh Y, Dastmalchi S, Mohammadi G, Niri FK, Alaei-Beirami M. Naproxen-eudragit RS100 nanoparticles: preparation and physicochemical characterization. Colloids Surf B Biointerfaces. 2011;83(1):155-159.
21. Yadav B, Chauhan M, Sonali, Dinkar R, Shekhar S, Monika, et al. In silico modeling, development, characterization, in-vitro cytotoxicity, pharmacokinetic, and toxicological studies of folate-receptor targeted micelles containing cisplatin and upconversion nanoparticles for lung cancer therapy. Mater Today Commun. 2024;39:109007.
22. Vaculikova E, Placha D, Pisarcik M, Peikertova P, Dedkova K, Devinsky F, et al. Preparation of risedronate nanoparticles by solvent evaporation technique. Molecules. 2014;19(11):17848-17861.
23. Anjum MM, Patel KK, Dehari D, Pandey N, Tilak R, Agrawal AK, et al. Anacardic acid encapsulated solid lipid nanoparticles for Staphylococcus aureus biofilm therapy: chitosan and DNase coating improves antimicrobial activity. Drug Deliv Transl Res. 2021;11(1):305-317.
24. Salatin S, Barar J, Barzegar-Jalali M, Adibkia K, Kiafar F, Jelvehgari M. Development of a nanoprecipitation method for the entrapment of a very water soluble drug into Eudragit RL nanoparticles. Res Pharm Sci. 2017;12(1):1-14.
25. Pawar P, Duduskar A, Waydande S. Design and evaluation of Eudragit RS-100 based itraconazole nanosuspension for ophthalmic application. Curr Drug Res Rev. 2021;13(1):36-48.
26. Katara R, Majumdar DK. Eudragit RL 100-based nanoparticulate system of aceclofenac for ocular delivery. Colloids Surf B Biointerfaces. 2013;103:455-462.
27. Chauhan M, Sonali, Shekhar S, Yadav B, Garg V, Dutt R, et al. AS1411 aptamer/RGD dual functionalized theranostic chitosan-PLGA nanoparticles for brain cancer treatment and imaging. Biomater Adv. 2024;160:213833.
28. Shafiei F, Ghavami-Lahiji M, Jafarzadeh Kashi TS, Najafi F. Drug release kinetics and biological properties of a novel local drug carrier system. Dent Res J (Isfahan). 2021;18:94.
29. Bhasarkar J, Bal D. Kinetic investigation of a controlled drug delivery system based on alginate scaffold with embedded voids. J Appl Biomater Funct Mater. 2019;17(2):2280800018817462.
30. Jeyamohan P, Hasumura T, Nagaoka Y, Yoshida Y, Maekawa T, Kumar DS. Accelerated killing of cancer cells using a multifunctional single-walled carbon nanotube-based system for targeted drug delivery in combination with photothermal therapy. Int J Nanomedicine. 2013;8:2653-2667.
31. Zhang S, Wang C. Precise Analysis of nanoparticle size distribution in TEM image. Methods Protoc. 2023;6(4):63.
32. Poidevin C, Paciok P, Heggen M, Auer AA. High resolution transmission electron microscopy and electronic structure theory investigation of platinum nanoparticles on carbon black. J Chem Phys. 2019;150(4):041705.
33. Yenilmez E. Desloratadine-eudragit® RS100 nanoparticles: formulation and characterization. Turk J Pharm Sci. 2017;14(2):148-156.
34. Salatin S, Barar J, Barzegar-Jalali M, Adibkia K, Kiafar F, Jelvehgari M. Development of a nanoprecipitation method for the entrapment of a very water soluble drug into Eudragit RL nanoparticles. Res Pharm Sci. 2017;12(1):1-14.
35. Khan F, Katara R, Ramteke S. Enhancement of bioavailability of cefpodoxime proxetil using different polymeric microparticles. AAPS PharmSciTech. 2010;11(3):1368-1375.
36. Işık M, Levorse D, Mobley DL, Rhodes T, Chodera JD. Octanol-water partition coefficient measurements for the SAMPL6 blind prediction challenge. J Comput Aided Mol Des. 2020;34(4):405-420.
37. Heredia NS, Vizuete K, Flores-Calero M, Pazmiño V K, Pilaquinga F, Kumar B, Debut A. Comparative statistical analysis of the release kinetics models for nanoprecipitated drug delivery systems based on poly(lactic-co-glycolic acid). PLoS One. 2022;17(3):e0264825.
38. Kaegi R, Fierz M, Hattendorf B. Quantification of Nanoparticles in Dispersions Using Transmission Electron Microscopy. Microsc Microanal. 2021:1-9.

39. Kamiya M, Matsumoto M, Yamashita K, Izumi T, Kawaguchi M, Mizukami S, Tsurumaru M, Mukai H, Kawakami S. Stability Study of mRNA-Lipid Nanoparticles Exposed to Various Conditions Based on the Evaluation between Physicochemical Properties and Their Relation with Protein Expression Ability. Pharmaceutics. 2022;14(11):2357.
40. Phan HT, Haes AJ. What does nanoparticle stability mean? J Phys Chem C Nanomater Interfaces. 2019;123(27):16495-16507.
41. Sharma A, Keservani R, Dadarwal S, Choudhary Y, Ramteke S. Formulation and in vitro characterization of cefpodoxime proxetil gastroretentive microballoons. Daru.;19(1):33-40.
42. Fu Y, Kao WJ. Drug release kinetics and transport mechanisms of non-degradable and degradable polymeric delivery systems. Expert Opin Drug Deliv. 2010;7(4):429-444.
43. Dikpati A, Maio VDP, Ates E, Greffard K, Bertrand N. Studying the stability of polymer nanoparticles by size exclusion chromatography of radioactive polymers. J Control Release. 2024;369:394-403.
44. Chauhan M, Sonali, Shekhar S, Yadav B, Garg V, Dutt R, et al. AS1411 aptamer/RGD dual functionalized theranostic chitosan-PLGA nanoparticles for brain cancer treatment and imaging. Biomater Adv. 2024;160:213833.
45. Singh RP, Sonali. Current Trends and Challenges in Targeting Tumor Mitochondrial Glycolysis and Oxidative Phosphorylation Pathways for Cancer Therapy. Curr Protein Pept Sci. 2025;26(1):2-5.
46. Chauhan M, Singh RP, Sonali, Yadav B, Shekhar S, Kumar L, Mehata AK, Jhawat V, Dutt R, Garg V, Kailashiya V, Muthu MS. Dual-targeted transferrin and AS1411 aptamer conjugated micelles for improved therapeutic efficacy and imaging of brain cancer. Colloids Surf B Biointerfaces. 2023;231:113544.